Infrared reflectance and transmission spectra in II-VI alloys and superlattices

Devki N. Talwar*
Department of Physics, Indiana University of Pennsylvania, 975 Oakland Avenue, 56 Weyandt Hall, Indiana, Pennsylvania 15705-1087, USA

Tzuen-Rong Yang
Department of Physics, National Taiwan Normal University, Taipei 106-11, Taiwan, ROC

Zhe Chuan Feng
Institute of Photonics & Optoelectronics and Department of Electrical Engineering, National Taiwan University, Taipei 106-17, Taiwan, ROC

P. Becla
Department of Materials Science and Engineering, Massachusetts Institute of Technology, Cambridge, Massachusetts 02139, USA
(Received 20 June 2011; revised manuscript received 25 August 2011; published 8 November 2011)

Room temperature measurements of the far-infrared (FIR) reflectance spectra are reported for the polar optical phonons in a series of bulk $Cd_xZn_{1-x}Te$ ($0 \leqslant x \leqslant 1$) and $CdSe_xTe_{1-x}$ ($0 < x \leqslant 0.35$) crystals grown by Bridgman technique. The composition-dependent spectra exhibited many fundamental aspects of lattice vibrations, while the results of long-wavelength optical modes for the end member binary compounds displayed phonon values in good agreement with the existing inelastic neutron scattering and/or Raman spectroscopy data. Using a standard methodology of multilayer optics with effective-medium dielectric tensors, we simulated the FIR transmission and reflectivity spectra at oblique incidence (Berreman's effect) in many II-VI free-standing thin films, epilayers and superlattices. Berreman's approach provided us with a strong basis for analyzing the infrared experimental data and offered an effective means of estimating the zone-center transverse and longitudinal optical (ω_{TO}, ω_{LO}) phonon frequencies in polar-semiconductor thin films and heterostructure materials of increasing technological importance.

DOI: 10.1103/PhysRevB.84.174203 PACS number(s): 78.20.−e, 63.20.Pw, 63.20.D−

I. INTRODUCTION

The optical, structural, and electrical properties of luminescent II-VI compound semiconductors[1–14] with band-gap energies ranging from 0 to 4 eV are appealing for ultrasensitive multiplexing/multicolor applications in a variety of emerging areas of biotechnology, nanoscale optoelectronics, and nanophotonics.[8–14] By varying the composition and controlling the lattice constants in ternary or quaternary alloys, we can achieve greater flexibility of tuning emission and absorption wavelengths for high-efficiency solid-state light emission sources.[15–27] Earlier, the applications of II-VI materials for photonic devices were hampered primarily by the availability of poor-quality crystals and the difficulty of managing doping.[28–33] Progress in the modern crystal growth techniques such as metalorganic vapor phase epitaxy (MOVPE),[34] metalorganic chemical vapor deposition,[35] molecular beam epitaxy (MBE),[36,37] chemical beam epitaxy,[38] and hot wall epitaxy[39] has offered higher quality and greater versatility in the preparation of thin films with controlled doping on many convenient substrates.[40–42] The ability to prepare zinc–cadmium (mercury)–based binary [AB, with A = Zn, Cd, and Mn (Hg) and B = S, Se, and Te] compounds[43–45] and thin films of ternary $A_{1-x}B_xC$ (e.g., $Cd_{1-x}Zn_xTe$, $CdTe_{1-x}Se_x$, etc.) or quaternary $A_{1-x-y}B_xC_yD$ (e.g., $Cd_{1-x-y}Zn_xMn_yTe$, $CdSe_xS_yTe_{1-x-y}$, etc. where C and D can be the elements of the binary compound AB) alloys with precise chemical compositions x, y has now opened up many possibilities of using II-VI materials in various technological applications. Both MOVPE and MBE techniques are capable of producing thin films of different compounds and crystal structures that are not the lowest-energy configurations in bulk materials. For instance, both CdTe and ZnTe exhibit in the zinc-blende phase, while bulk CdS and CdSe reveal wurtzite crystal structures. The later compounds can be grown, however, in thin-film forms on GaAs (100) substrates,[46,47] where the fourfold periodicity of the underlying layer causes adoption of the metastable zinc-blende structure for CdS and CdSe rather than their lower-energy wurtzite phase. These characteristics have injected many excitements to the crystal growth community,[34–47] providing opportunities to design a variety of lattice-matched heterostructure materials and to fabricate various devices for optoelectronics and integrated optics.

Apart from bulk materials, II-VI–based thin films, epilayers, ternary alloys, and superlattice (SL) structures grown on various substrates have presented strong interest in many applications, including photonics, photoconduction, photovoltaic, x-ray detectors for medical imaging, and diagnostics.[48–52] While the high-absorption coefficient of $Cd_{1-x}Zn_xTe$ has made it enviable for room temperature x-ray and γ-ray detectors, the band gap of ∼1.5 eV of CdTe is perfectly matched to the distribution of photons in the solar spectrum for its use in the high-efficiency photovoltaic cells.[53–55] Despite the significance of II-VI epilayers, alloys, and low-dimensional systems for optic and photonic applications,[48–55] only a limited number of investigations have been carried out of their basic properties[56–68] especially the physics behind those characteristics that determine the importance of such materials at a practical level. To a large degree, many fundamental

properties of the epitaxially grown II-VI materials depend upon their lattice dynamics and electron–phonon interaction.[69–73] Scattering of thermal neutrons by solids[56] (e.g., ZnS, ZnSe, ZnTe, and CdTe) is by far the most useful tool for studying lattice vibrations, since their interaction extends over almost the entire range of energies and wave vectors in the Brillouin zone. Unfortunately, the neutron scattering method cannot be applied to thin films or nanostructured materials (SLs and/or quantum wells, etc.) because the available epitaxially grown samples are too lean to obtain measurable signals to resolve modes and branches of the phonon dispersions lying very close in frequency. On the other hand, besides the conventional use of determining vibrational frequencies, the far-infrared (FIR)[74–85] reflectance/transmission spectroscopy and Raman scattering[86–90] have shown excellent capabilities of measuring many electrical and structural parameters of semiconductor thin-film alloys, including layer thickness, free-carrier concentration, scattering time, and composition x. Although a significant amount of published work exists on Cd-Zn chalcogenides—dealing mostly with the specimen[53–55] preparation and measuring electronic and structural properties—the studies of lattice dynamics, elastic, and thermodynamic properties in their zinc-blende phase are either scarcely known[59] or contradictory.[68] Acquiring the correct knowledge of phonon dispersions in II-VI compound semiconductors is crucial *per se* for the characterization of free-standing chalcogenide thin films, ternary alloys, and epitaxially grown heterostructural materials and devices. In the framework of a realistic rigid-ion model, it has been possible to describe accurately the structural, phonon, and lattice dynamics properties of both perfect and imperfect compound semiconductors.[91–97]

The purpose of the present work is to report the results of a comprehensive theoretical and experimental investigation for the vibrational properties of bulk Cd-Zn chalcogenides, ternary alloys, and their SLs. By using a Fourier transform infrared (FTIR) spectroscopy, we have portrayed our room temperature results of the polar optical phonons for $Cd_{1-x}Zn_xTe$ ($0 < x < 1$) and CdS_xTe_{1-x} ($0 < x \leqslant 0.35$) alloys (c.f. Sec. II) grown by Bridgman technique. A succinct description of the dielectric response theory is outlined in Sec. III A for studying the FIR reflectance at near-normal incidence in bulk semiconductor alloys, thin films, and heterostructures. In Sec. III B, we delineate a standard methodology of the multilayer optics to examine the FIR reflectance and transmission spectra[85] at oblique incidence (Berreman effect[82]) in thin epilayers (see Fig. 1) and SLs (see Fig. 2). The experimental results are analyzed (c.f. Sec. IV) by using parameters derived from the realistic lattice dynamics scheme,[98] providing valuable information on the structural identity and crystalline quality of the material samples. Theoretical calculations of the reflectance spectra at normal incidence in $Cd_xZn_{1-x}Te$ ($0 < x < 1$) and $CdTe_{1-x}Se_x$ ($0 < x \leqslant 0.35$) ternary alloys (c.f. Sec. IVA) are found to agree well with our experimental data. In Berreman's effect, if the wavelength λ of the FIR radiation incident at an angle θ on a film of thickness d (with $d \ll \lambda$) has an electric vector polarized perpendicular to the plane of incidence (c.f. Fig. 1), there occurs *one* transmission T_s (s-polarization) minimum at the transverse optical (TO) mode; for an electric vector polarized parallel to the plane of incidence, there are *two* transmission T_p

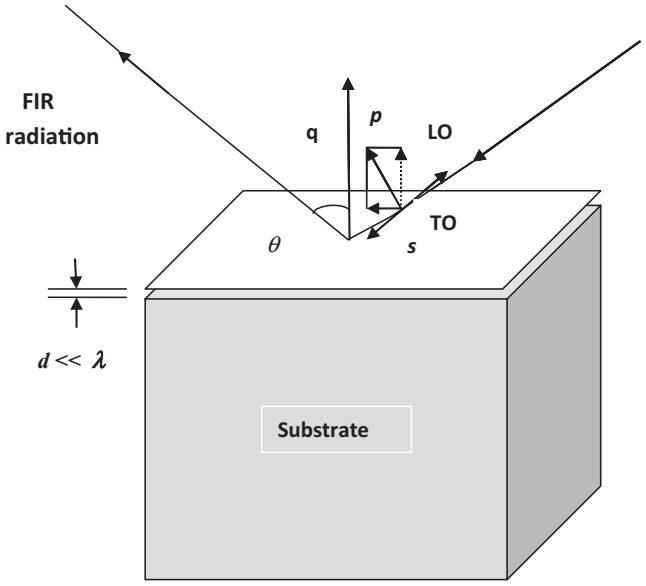

FIG. 1. Polar semiconductor thin film grown on a thick substrate. The directions of the s (perpendicular, $\perp$) and p (parallel, $\parallel$) components of the FIR radiation incident are at an oblique angle to the surface of a thin film (perpendicular to the phonon wave-vector $\vec{q}$) of thickness $d \ll \lambda$ grown on a thick substrate.

(p-polarization) minima observed at the TO and longitudinal optical (LO) modes.[83–85] At normal incidence, on the other hand, only one transmission minimum at the TO frequency is observed independent of the polarization. Consistent with the experimental results (c.f. Sec. IV B), our calculations of the FIR transmission and reflection spectra in the s- and p-polarization for the free-standing CdTe thin films, CdSe/GaAs epilayers, and $(CdSe)_m/(ZnTe)_n$ SLs have provided strong revelations of the distinct minima corresponding to the TO, TO, and LO phonons, respectively. Results of the numerical simulations are compared and discussed with the existing FIR reflectivity/transmission spectra in Sec. IV, with concluding remarks presented in Sec. V.

II. EXPERIMENTAL DETAILS

A. $CdSe_xTe_{1-x}$ and $Cd_{1-x}Zn_xTe$ ternary alloys

The material samples used in the present study were grown at the Massachusetts Institute of Technology using the Bridgman technique. The $CdSe_xTe_{1-x}$ ($0 < x \leqslant 0.35$) and $Cd_xZn_{1-x}Te$ ($0 < x < 1$) ternary alloys were prepared by reacting the 99.9999% pure elemental constituents in the evacuated sealed quartz tubes $\sim$1150 °C. The composition values x determined from the mass densities, and the precast alloys were thin films by directional solidification at the rates of 0.8–1 mm/h for $CdSe_xTe_{1-x}$ and 1.2 mm/h for $Cd_xZn_{1-x}Te$ in a Bridgman-Stockbarger–type furnace. The resultant boules cut into slices, 1–2 mm thick, perpendicular to the growth axis were annealed at 650 °C in a Se-saturated or Cd-saturated atmosphere to improve the crystalline perfection. Finally, the sample surfaces were prepared by lapping, mechanical polishing, and etching in a bromine–methanol solution. The alloy composition set by the ratio of constituents before growth was confirmed by the x-ray diffraction and transmission

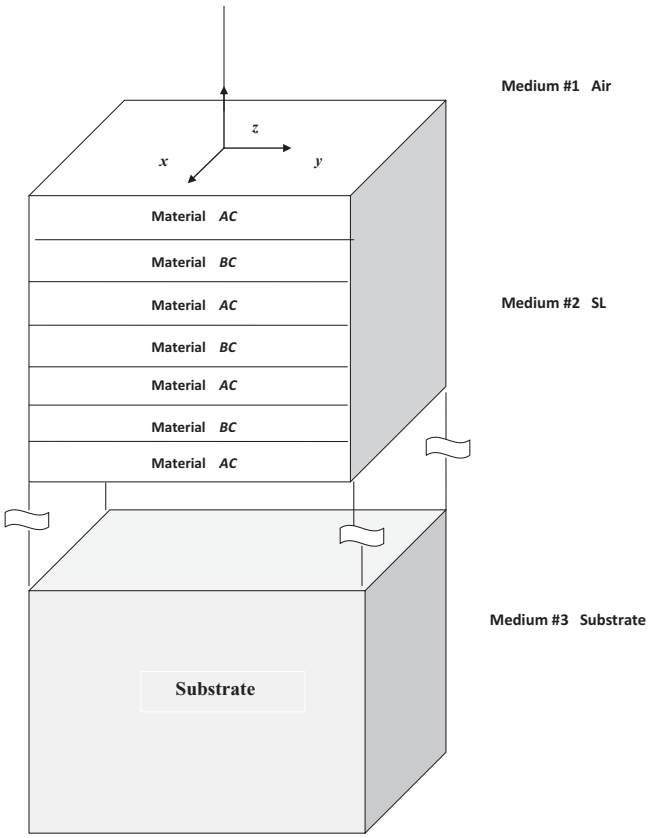

FIG. 2. Polar semiconductor SL grown on a thick substrate. The polar semiconductor SL structure consists of two optically isotropic layers (*AC* and *BC*) of thickness d_{AC} and d_{BC} consisting of repeat period p grown alternately on a thick substrate.

measurements after preparation. All samples were found to be single crystal with the zinc-blende structure.

B. FIR reflectivity

The room temperature FIR reflectance spectra for $Cd_xZn_{1-x}Te$ ($0 < x < 1$) and $CdTe_{1-x}Se_x$ ($0 < x \leqslant 0.35$) samples at near-normal incidence (see Figs. 3 and 4) were measured at the National Taiwan Normal University. We used a Bruker IFS66 spectrometer with KBr beam splitter and a deuterated triglycine sulfate detector to achieve the good signal-to-noise ratio in the spectral range 40–250 cm^{-1} at a resolution of $\sim$0.1 cm^{-1}. The incident angle was set $\sim 9^\circ$—a negligible deviation from the near-normal incidence. The reflection coefficient was measured by rationing the intensity of the light reflected from the sample against that reflected from a reference mirror made of a silver coin with about 99% reflectance. Since the masses of Cd and Zn in $Cd_xZn_{1-x}Te$ are quite different from those of Se and Te in $CdTe_{1-x}Se_x$ alloys, we expected the vibrational spectra in the two-semiconductor-material systems to be qualitatively distinctive. The measured FIR reflectance spectra of all $Cd_xZn_{1-x}Te$ and $CdTe_{1-x}Se_x$ samples were analyzed theoretically in terms of an effective dielectric function with optical constants (see Table I) using the classical Drude-Lorentz oscillators (c.f. Sec. IIIA), representing the lattice and free-carrier contributions. The results of a modified random-isodisplacement (MREI) model

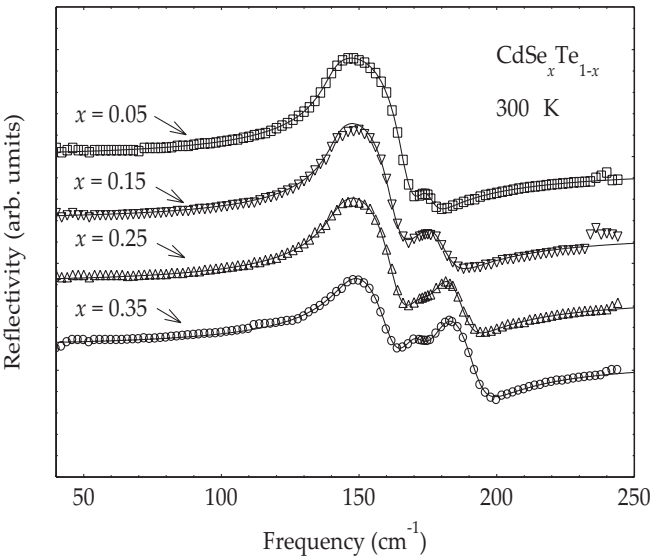

FIG. 3. Room temperature FTIR reflectivity spectra for bulk $CdSe_xTe_{1-x}$ ($x = 0.05$, 0.15, 0.25, and 0.35) samples grown by the Bridgman technique.

describing the behavior of optical phonons in $Cd_{1-x}Zn_xTe$ and $CdTe_{1-x}Se_x$ with x are shown in Fig. 5.

III. THEORETICAL CONSIDERATIONS

Optoelectronic devices based on II-VI compound semiconductor alloys and their multilayer structures are generally composed of various thin homo- or heterofilms of different thicknesses, compositions, and doping levels.[1–14] Such novel metastable materials, unavailable in nature, are being prepared by modern epitaxial growth techniques.[34–42] Understanding their physical properties in the context of controlling parameters (viz. the band gaps, lattice constants, compositions, and

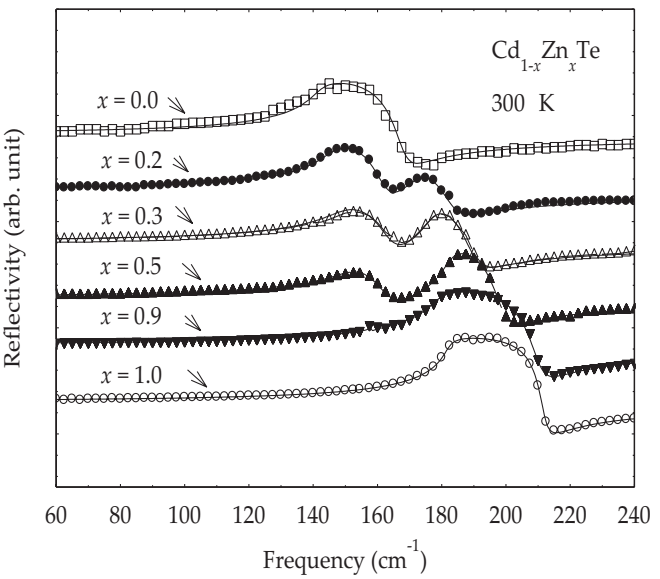

FIG. 4. Room temperature FTIR reflectivity spectra of bulk $Cd_{1-x}Zn_xTe$ ($x = 0.2$, 0.3, 0.5, 0.9, and 1.0) samples grown by the Bridgman technique.

TABLE I. Optical parameters fitted by the dielectric response model for (a) $Cd_{1-x}Zn_xTe$ and (b) $CdSe_xTe_{1-x}$ ternary alloys in the long-wavelength limit.

(a) $Cd_{1-x}Zn_xTe$		CdTe-like mode			ZnTe-like mode			Mixed mode		
x	ε_∞	S_1	ω_{TO1}	Γ_1	S_2	ω_{TO2}	Γ_2	S_3	ω_{TO3}	Γ_3
0.0	8.52	3.7	141.7	8.63						
0.2	8.17	3.2	145.6	9.28	0.45	171.73	10.86			
0.3	7.96	2.90	149.2	12.9	0.64	176.52	7.3			
0.5	7.81	2.2	152.0	13.72	0.93	182.07	5.6			
0.9	7.05	0.15	158	15.0	2.33	182.0	3.99			
1.0	6.91				3.14	182.5	3.33			
(b) $CdSe_xTe_{1-x}$		CdTe-like mode			CdSe-like mode			Mixed mode		
x	ε_∞	S_1	ω_{TO1}	Γ_1	S_2	ω_{TO2}	Γ_2	S_3	ω_{TO3}	Γ_3
0.05	8.59	4.05	140.06	8.63	0.054	174.0	7.54			
0.15	8.74	3.81	141.81	8.03	0.28	178.67	17.16	0.057	174.48	10.11
0.25	8.86	3.94	142.25	10.43	0.33	180.42	11.32	0.096	172.0	10.11
0.35	9.07	3.53	145.46	12.89	0.55	180.42	11.83	0.25	170.0	9.76

valence band offsets in quantum well structures) have created significant interests and challenges for their use in designing novel materials and devices. From an experimental standpoint, the detailed information about the lattice vibrations of any perfect or imperfect crystal can be obtained using optical methods that measure the frequency-dependent response to an external probe. The inelastic coherent neutron scattering method, the most efficient means to reveal the normal modes in bulk materials, has not been applied, to the best our knowledge, to cubic phase of CdSe. On the other hand, FIR spectroscopy and Raman scattering data available in recent years can be used to understand the structural and vibrational properties of $CdTe_{1-x}Se_x$ alloys and CdSe/ZnTe SLs.[74–85]

A. Classical theory of FIR reflection at normal incidence

In the FIR region, the physical processes involved in crystal lattices can be described by the interactions between radiation and matter. This interaction is articulated by the wave vector and frequency-dependent dielectric response function $\tilde{\varepsilon}(\omega,\vec{q})$. In zinc-blende-type polar semiconductor materials, two main processes contribute to $\tilde{\varepsilon}(\omega,\vec{q})$: (1) the free-carrier effect $[\tilde{\varepsilon}_e(\omega,\vec{q})]$ from the electrons in the conduction band or from the holes in the valence band and (2) the lattice effect $[\tilde{\varepsilon}_i(\omega,\vec{q})]$ from the optical phonons.[74–81,99] In the limiting case, where the wave-vector $\vec{q}$ approaches to zero, the general form of the dielectric function in classical model takes the form

$$\tilde{\varepsilon}(\omega) = \tilde{\varepsilon}_e(\omega) + \tilde{\varepsilon}_i(\omega) \tag{1}$$

with

$$\tilde{\varepsilon}(\omega) = \varepsilon_\infty \left[1 - \frac{\omega_p^2}{\omega(\omega + i\gamma)}\right] + \frac{S\omega_{TO}^2}{\left(\omega_{TO}^2 - \omega^2 - i\Gamma\omega\right)}, \tag{2}$$

where, the term $\omega_p = \sqrt{\frac{4\pi\eta e^2}{m_e^*\varepsilon_\infty}}$ in Eq. (2) represents the plasma frequency, η stands for the free-carrier density, m_e^* is the effective mass, γ (Γ) signifies the plasmon (phonon) damping coefficient, ω_{TO} symbolizes the TO phonon frequency, and S is the oscillator strength. Calculation of the dielectric function in semiconductor materials is the foundation of relating phonon frequencies to the FIR reflectivity spectrum.

1. Bulk ternary alloys

In a zinc-blende-type polar semiconductor ternary alloy (e.g., $A_{1-x}B_xC$), the complex dielectric function (Eq. (2)) can be rewritten as

$$\tilde{\varepsilon}(\omega) = \varepsilon_{\infty x}\left[1 - \frac{\omega_p^2}{\omega(\omega + i\gamma)}\right] + \sum_{j=1,2} \frac{S_{jx}\omega_{TOxj}^2}{\omega_{TOjx}^2 - \omega^2 - i\Gamma_{jx}\omega}, \tag{3}$$

where, the term ε_{∞_x} represents the high-frequency dielectric constant taken as a weighted average between the corresponding values of the pure binary compounds *AC*-*BC*, S_{jx} is the oscillator strength, ω_{TOjx} and Γ_{jx} represent, respectively, the resonance frequency and the damping parameters of the *j*th TO phonon for different composition x.

In general, the dielectric function of the alloy $\tilde{\varepsilon}(\omega)[= \varepsilon_1(\omega) + i\varepsilon_2(\omega)]$ can be separated into the real $[\varepsilon_1(\omega)]$ and imaginary $[\varepsilon_2(\omega)]$ parts, where $\varepsilon_2(\omega)$ represents the absorption of energy as a function of frequency and therefore affects directly the reflectivity spectrum of the material. The dielectric function $\tilde{\varepsilon}(\omega)$ can also be related to the real and imaginary parts of the complex refractive index, $\tilde{n}[= n + i\kappa] = \sqrt{\tilde{\varepsilon}}$:

$$n^2 - \kappa^2 = \varepsilon_1, \tag{4a}$$

$$2n\kappa = \varepsilon_2, \tag{4b}$$

where the optical constants n and κ are the index of refraction and the extinction coefficient, respectively. Once the dielectric function is known, the reflectance coefficient $\tilde{r}$,

$$\tilde{r} = \left(\frac{1 - \sqrt{\tilde{\varepsilon}}}{1 + \sqrt{\tilde{\varepsilon}}}\right), \tag{5a}$$

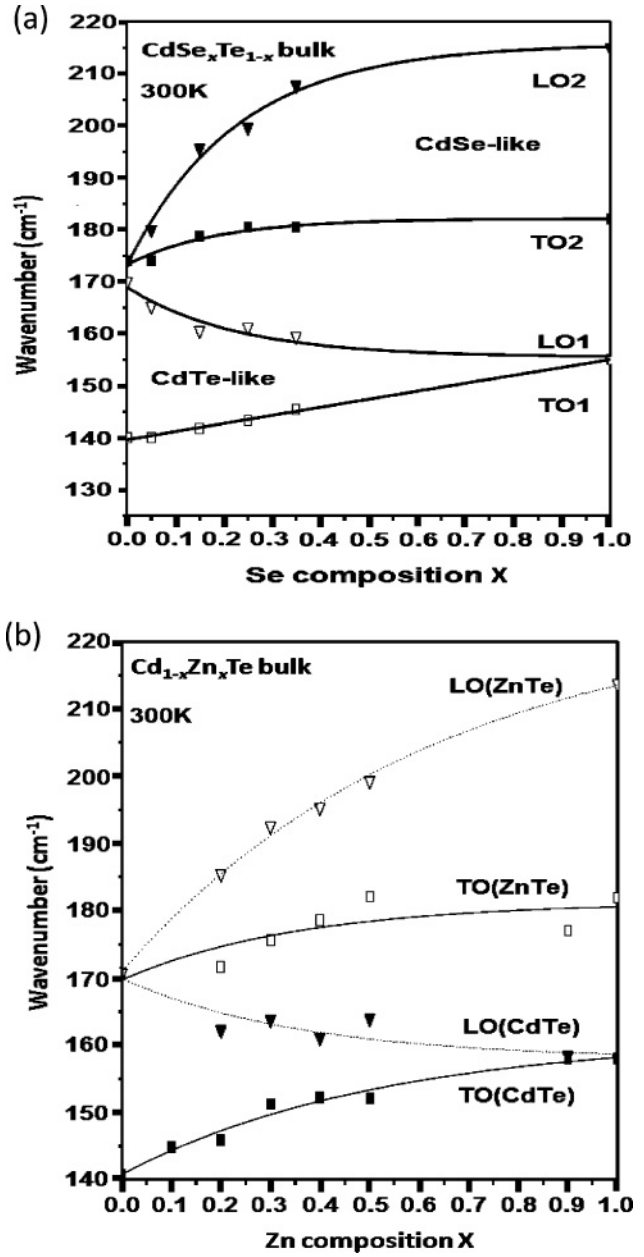

FIG. 5. Variation of experimental results of optical phonon frequency (cm^{-1}) versus x for (a) $CdSe_xTe_{1-x}$ (▼■▽□) and (b) $Cd_{1-x}Zn_xTe$ (▼■▽□). The solid lines are the results based on the MREI model.

and hence the power reflection $R(\omega)$ at normal incidence

$$R(\omega) = |\tilde{r}|^2 , \tag{5b}$$

for semiconductor alloys can be calculated.

2. *Thin films, epilayers, and/or heterostructures*

As the penetration depth of the FIR radiation is $\sim 3\ \mu$m in nontransparent materials, the reflectivity in a polar thin film and/or heterostructure of thickness much smaller than 3 μm is expected to provide structural information of its constituents and the substrate on which the material is grown. Once the dielectric functions of the binary or ternary alloys are known, the reflection and transmission spectra of thin films, epilayers, and/or SLs can be easily obtained.

To treat the reflectance and transmission of a thin film grown on a substrate (c.f. Fig. 1), we adopted a three-medium "air–film–substrate" system with dielectric functions $\varepsilon_1 = 1$ (air), $\varepsilon_2 = \tilde{\varepsilon}_{tf}$(thin film), and $\varepsilon_3 = \tilde{\varepsilon}_s$(substrate). Following Cadman and Sadowski,[100] the reflection $\tilde{r}_{123}$ and transmission $\tilde{t}_{123}$ coefficients at normal incidence for such an epilayer of thickness d can be written as

$$\tilde{r}_{123} = \frac{\tilde{r}_{12} + \tilde{r}_{23}\exp[i2\beta]}{1 + \tilde{r}_{12}\tilde{r}_{23}\exp[i2\beta]}, \tag{6a}$$

$$\tilde{t}_{123} = \frac{(1 + \tilde{r}_{12})(1 + \tilde{r}_{23})\exp[i2\beta]}{1 - \tilde{r}_{12}\tilde{r}_{23}\exp[i2\beta]}, \tag{6b}$$

where $\tilde{r}_{ij} = \frac{\tilde{n}_i - \tilde{n}_j}{\tilde{n}_i + \tilde{n}_j}$ are the Fresnel coefficients and $\beta = 2\pi d\omega\sqrt{\tilde{\varepsilon}_2}$ is a phase multiplier. The power reflection $R(\omega)$ and transmission $T(\omega)$ are simply given by

$$R(\omega) = |\tilde{r}_{123}|^2 \tag{7a}$$

$$T(\omega) = |\tilde{t}_{123}|^2 . \tag{7b}$$

In an effective medium theory, the preceding approach for thin films can be extended to the SL structure displayed in Fig. 2. The dielectric function $\tilde{\varepsilon}_{SL}$ of the SL is a diagonal tensor whose components in the long-wavelength limit can be written as weighted averages of the dielectric functions of the constituent layer materials. For the FIR radiation with electric field parallel to the layers, the $\tilde{\varepsilon}_{SL}$ in the effective medium approximation, takes the form

$$\tilde{\varepsilon}_{SL}(\omega) = \left[\frac{\tilde{\varepsilon}_{AC}(\omega)\delta + \tilde{\varepsilon}_{BC}(\omega)}{\delta + 1}\right], \tag{8}$$

where $\tilde{\varepsilon}_{AC}$ and $\tilde{\varepsilon}_{BC}$ are the dielectric functions of bulk materials AC and BC of the constituent layers forming the SL and $\delta = \frac{d_{AC}}{d_{BC}}$ is the ratio of thicknesses of the two alternating

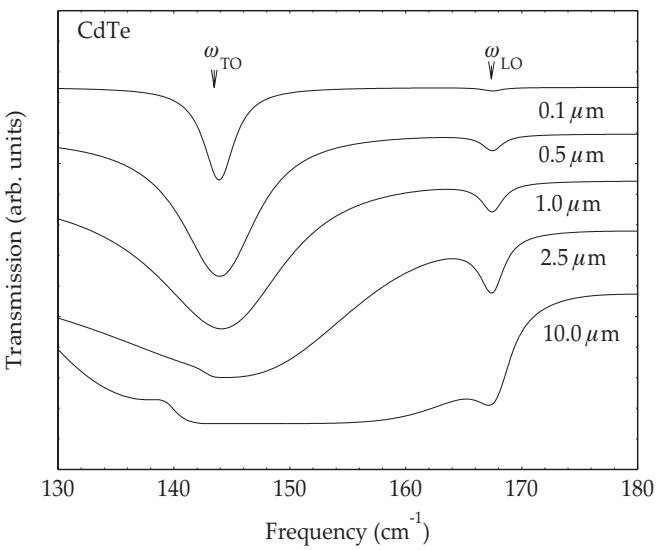

FIG. 6. Calculated transmission of the free-standing CdTe films as a function of frequency (cm^{-1}) in the p-polarization for $\theta_i = 45^\circ$ with increasing thicknesses. The spectra for films of different thickness are vertically displaced for clarity.

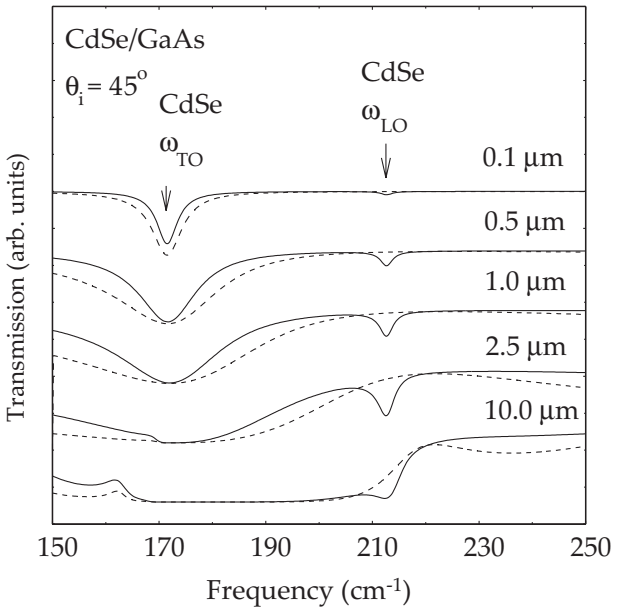

FIG. 7. Calculated transmission of CdSe/GaAs epilayers grown on GaAs substrate as a function of frequency (cm^{-1}) in the *s*-polarization (dotted line) and *p*-polarization (full line) for $\theta_i = 45^\circ$ with increasing thicknesses. The spectra for the films of different thickness are vertically displaced for clarity.

layers (c.f. Fig. 2). For oblique incidence, Eqs. (6a) and (7a) for studying the reflectance and transmission coefficients are no longer valid, because $R(\omega)$ and $T(\omega)$ become complicated functions of both the angle of incidence and the polarization (c.f. Sec. IIIB).

B. FIR reflection and transmission at oblique incidence

In the conventional FIR spectroscopy, the measurements of reflection and transmission at near-normal incidence are used to extract optical constants in compound semiconductors. Due to the transverse characteristics of the electromagnetic radiations, we expect to observe in polar materials only the zone-center TO phonons at normal incidence. In thin films, however, the interaction of electromagnetic field with the material can be enhanced by an oblique incidence. Using infrared (IR) spectroscopy (transmission or reflection) at an oblique incidence, Berreman[82] first predicted theoretically and demonstrated experimentally the observation of TO and LO phonons in LiF thin films grown on a collodion film. For *p*-polarized light, the LO structure is generated by the surface charges due to the normal component of the electric field. Many transmission measurements at oblique incidence have now been reported in the literature on a diverse group of II-VI free-standing thin films, epilayers, and SLs,[85] offering a direct ratification of the Berreman effect. More recently, the detection of the *p*-polarization minima associated with the TO phonon and the high-frequency LO phonon–plasmon–coupled L_+ modes has made the FIR transmission spectroscopy a highly sensitive tool for estimating the free-charge-carrier density in doped semiconductor thin films.[84,96] In the framework of a multilayer optics and using the effective medium dielectric tensor, we can simulate the transmission and reflection spectra at oblique incidence for free-standing thin films, epilayers, and SLs.

As mentioned earlier, the polar II-VI semiconductors exhibit distinct response to the FIR radiation between *s*- and *p*-polarization when the light is incident obliquely to the surface of the material. Here, the terms *s* and *p* imply the directions of the linear polarization that are perpendicular and parallel, respectively, to the plane of incidence. Berreman's argument consisted of the demonstration that for thin films ($d \ll \lambda$) the long-wavelength phonons have the wave-vector $\vec{q}$ perpendicular to the film surface such that the normal incidence radiation can interact only with the TO modes (parallel to the surface). On the other hand, the *p*-polarized component of the oblique incident radiation, as shown in Fig. 1, has subcomponents parallel and perpendicular to the film surface, which can excite TO and LO phonons, respectively.

Following Piro,[101] the analytical expressions for $R(\omega)$ and $T(\omega)$ at an arbitrary angle of incidence θ_i can be derived for an isotropic layer of thickness d grown on a thick isotropic substrate. The dielectric tensor $\tilde{\varepsilon}_{SL}$ of the SL consisting of two optically isotropic layers *AC*, *BC* grown alternately on a substrate (see Fig. 2) has the form of a uniaxial crystal of D_2d symmetry:

$$\tilde{\varepsilon}_{SL}(\omega) = \begin{bmatrix} \tilde{\varepsilon}_\perp & 0 & 0 \\ 0 & \tilde{\varepsilon}_\perp & 0 \\ 0 & 0 & \tilde{\varepsilon}_{||} \end{bmatrix}. \tag{9}$$

Here, the *z*-axis is set along the optical axis perpendicular to the plane of the SL. If the wavelength of the radiation is large compared to the period $d\ (= d_{AC} + d_{BC})$ of the SL, the electromagnetic boundary conditions give the values of $\tilde{\varepsilon}_\perp$ and $\tilde{\varepsilon}_{||}$:

$$\tilde{\varepsilon}_\perp(\omega) = \frac{\tilde{\varepsilon}_{AC}(\omega) d_{AC} + \tilde{\varepsilon}_{BC}(\omega) d_{BC}}{d_{AC} + d_{BC}} \tag{10a}$$

and

$$\tilde{\varepsilon}_{||}(\omega) = \frac{(d_{AC} + d_{BC})\tilde{\varepsilon}_{AC}(\omega)\tilde{\varepsilon}_{BC}(\omega)}{d_{AC}\tilde{\varepsilon}_{BC}(\omega) + d_{BC}\tilde{\varepsilon}_{AC}(\omega)}. \tag{10b}$$

For a SL grown on a thick substrate, the amplitude reflectance $\tilde{r}_{s(p)}$ (or amplitude transmittance $\tilde{t}_{s(p)}$) and hence the power reflectance $R_{s(p)}(\omega) = |\tilde{r}_{s(p)}|^2$ (or the power transmittance $T_{s(p)}(\omega) = |\tilde{t}_{s(p)}|^2$) can be obtained using

$$\tilde{r}_{s(p)} = \frac{(1-P)\cos Q - i(R-S)\sin Q}{(1+P)\cos Q - i(R+S)\sin Q}, \tag{11a}$$

$$\tilde{t}_{s(p)} = \left(\cos\xi - \frac{i}{2}\zeta \sin\xi\right)^{-1}; \tag{11b}$$

the terms P, Q, R, S, and ξ and ζ in the $s(p)$-polarization are given elsewhere.[98]

IV. NUMERICAL COMPUTATIONS RESULTS AND DISCUSSIONS

A. IR reflectivity at near-normal incidence

In Figs. 3 and 4, we displayed the results of our room-temperature measurement of the FIR reflectance spectra at near-normal incidence for four $CdTe_{1-x}Se_x$ ($0.35 \geqslant x > 0.05$)

and six samples of ternary $Cd_{1-x}Zn_xTe$ ($1 \geqslant x > 0$) alloys, respectively. The experimental data is synthesized theoretically in terms of an effective dielectric function (Eq. (2)) by the superposition of damped harmonic oscillator using appropriate optical constants (see Table I), e.g., the number of phonon modes, phonon frequencies oscillator strengths, and phonon damping. Most calculated attributes are found to be in good agreement with the observed FIR reflectance features.

In Fig. 4, we displayed several representative sets of our room temperature reflectance spectra for $Cd_{1-x}Zn_xTe$ ($x =$ 0.0, 0.2, 0.3, 0.5, 0.9, and 1.0). The FIR spectra of the alloys in the long-wavelength range are mainly modulated by the TO phonons. The $Cd_{1-x}Zn_xTe$ shows a typical of the "two-mode" system, where the two ($LO_i - TO_i$; $i = 1, 2$) zone-center optical phonons are characterized as the CdTe-like and ZnTe-like due to their obvious relationships to the reststrahlen bands with the gap ($ZnTe{:}Cd \approx 154$ cm^{-1}) and the local ($CdTe{:}Zn \approx 170$ cm^{-1}) modes occurring at the respective ends of the alloy systems. At $x = 0$, a broad band corresponding to the IR active mode of the pure CdTe is exhibited between 130 and 170 cm^{-1}, while for $x = 1$ a single band of bulk ZnTe is seen between 175 and 215 cm^{-1}. In the alloy sample with the composition $x = 0.9$, we see a weak but not clearly visible CdTe-like shoulder $\sim$155 cm^{-1}. As the composition x changes ($0.5 \rightarrow 0.3 \rightarrow 0.2$), the CdTe-like modes at the lower-energy side and the ZnTe-like modes at the higher-energy side become visible—clearly revealing the two-mode behavior for the alloy system.

In the $CdSe_xTe_{1-x}$ ($0.35 \geqslant x > 0.05$) alloy system, however, the zone-center optical phonons in the experimental reflectance spectra revealed a variety of behavior patterns depending upon the vibrational characteristics of the end members. We can note from Fig. 3 that for frequency < 170 cm^{-1} there are regular reststrahlen band characteristics of the CdTe-like TO phonon in all samples. As the Se composition in $CdTe_{1-x}Se_x$ increases, the band intensity of the CdTe-like TO mode decreases—its peak position shifts toward the higher-energy side, while the intensity of the CdSe-like TO mode increases, showing a split ($x > 0.05$) into an unresolved third band appearing between the CdTe-like and the CdSe-like TO modes for $x = 0.25$ and 0.35. It should be mentioned here that such a phonon behavior pattern is seen in several one- and two-mode-type ternary alloy systems and is likely to be the result of the $\vec{q}$-vector relaxation induced by alloy disorder.[95] The fluctuation of alloy potential in $CdTe_{1-x}Se_x$ removes the translational invariance of the lattice, causing the breakdown of the $\vec{q} = 0$ selection rule—thus allowing additional band to appear between the two TO phonon modes of the end members. The MREI approach in $CdTe_{1-x}Se_x$ alloys cannot account for the observed line shape changes because the model assumes an ideal effective medium that is perfectly homogenous at the local region and the statistical average of the neighboring atoms depends upon the composition x. To treat the vibrational characteristics of a "disordered" semiconductor alloy effectively, we have to choose either a percolation-based approach[102] or a microscopically averaged Green's function methodology.[93] Our calculations of the density of states using a comprehensive Green's function formalism[98] provided support to the observed additional band in $CdTe_{1-x}Se_x$ ($x > 0.05$) originating from a "nonrandom" alloy disorder. The results of an MREI model describing the behavior of optical phonons in $Cd_{1-x}Zn_xTe$ and $CdTe_{1-x}Se_x$ as a function of x are shown in Fig. 5. The frequencies of TO_2 and LO_2 modes determined from the MREI model in $CdTe_{1-x}Se_x$ for $x = 1, 0$ are consistent with the values obtained from the lattice dynamics calculations of phonons for the CdSe and CdTe crystals with the zinc-blende crystal structure.[98]

B. IR reflection and transmission at oblique incidence

The IR transmission/reflection spectra at oblique incidence ($\theta_i = 45^\circ$) for free-standing thin films, epilayers, and SLs grown on different substrates with increasing film thickness can be calculated following the procedure described in Sec. III. In thin polar materials ($d \ll \lambda$), as anticipated by theory and verified experimentally (Berreman's effect[82]), only TO phonons in the s-polarization and TO, LO phonons in the p-polarization are expected from the transmission/reflection spectra at oblique incidence. Here, we illustrate and discuss our simulation results of the transmission and reflection spectra at oblique incidence for thin semiconductor films and multilayer structures by using the methodology described in Sec. III B. The presentation of our calculations for the free-standing CdTe film (c.f. Sec. IV B 1), CdSe/GaAs (001) epilayers (c.f. Sec. IV B 2), and $(CdSe)_m/(ZnTe)_n$/GaAs (001) SL (c.f. Sec. IV B 3) provides a strong basis for analyzing the FIR experimental data and offers an alternative and effective means of determining optical phonon frequencies in technologically important polar heterostructure materials prepared by the epitaxial techniques.

1. CdTe free-standing films

Following the method of Sec. III and using the optical constants of CdTe (see Table I), we display in Fig. 6 the calculated results of the transmission spectra at oblique incidence $\theta_i = 45^\circ$ in the p-polarization for free-standing CdTe thin films with varying thickness. The results revealed transmission dips near $\omega_{TO} = 142$ cm^{-1} and $\omega_{LO} = 169$ cm^{-1} frequencies in very good agreement with the existing inelastic neutron scattering[56] and Raman spectroscopy[85] data. The study clearly demonstrated the progression from the two transmission dips for ultrathin films to a broad region of transmission covering the entire reststrahlen band for relatively thick films. Again, as the CdTe film thickness increases, we see interference fringes emerging below the TO frequency region for thick films—caused primarily by the rapid increase in the dielectric function $\tilde{\varepsilon}(\omega)$ for frequencies lying close to the pole at ω_{TO}.

2. CdSe/GaAs (001) epilayers

The CdSe films grown on (001) GaAs by MBE techniques are known to possess zinc-blende structures.[46] The perusal of Fig. 7 reveals our results of the transmission spectra in CdSe epilayers at oblique incidence ($\theta_i = 45^\circ$) with increasing film thickness—exhibiting TO phonon in the s-polarization and TO, LO modes in the p-polarization at frequencies near $\omega_{TO} = 172$ cm^{-1} and $\omega_{TO} = 172$ cm^{-1}, $\omega_{LO} = 213$ cm^{-1}, respectively. Clearly, the LO phonon frequency measured by the Raman spectroscopy near $\omega_{LO} = 212.6$ cm^{-1} is in very good agreement[85] with the value derived from the transmission

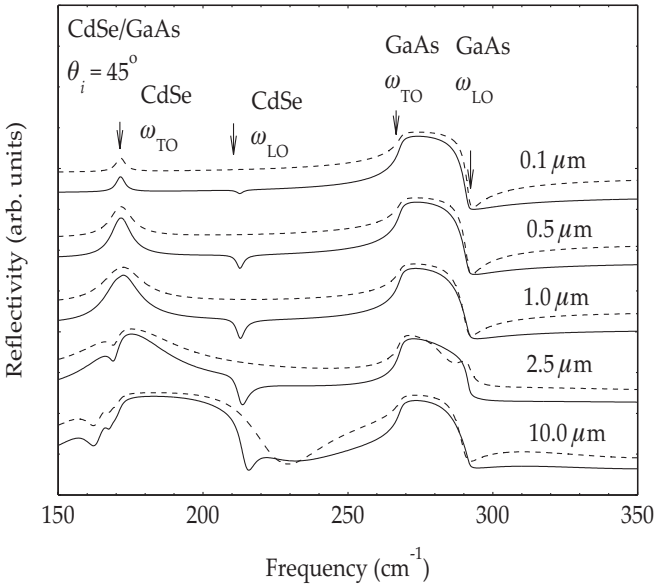

FIG. 8. Calculated reflectivity of CdSe/GaAs epilayers grown on GaAs substrate as a function of frequency (cm^{-1}) in the *s*-polarization (dotted line) and *p*-polarization (full line) for $\theta_i = 45^\circ$ with increasing thicknesses. The spectra for the films of different thickness are vertically displaced for clarity.

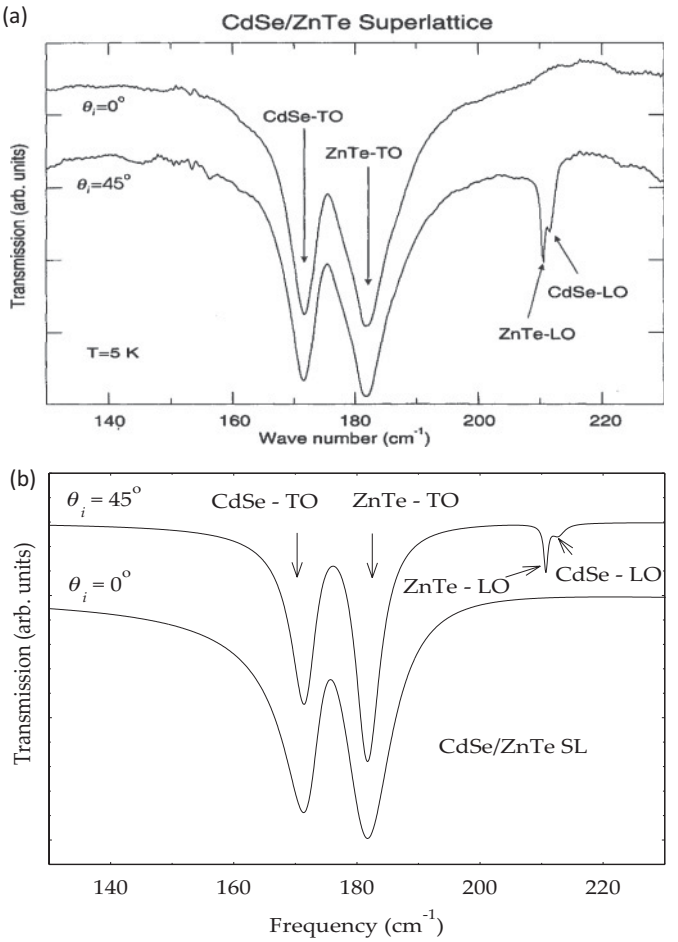

FIG. 9. Comparison of the transmission spectra for a CdSe/ZnTe SL grown on GaAs substrate as a function of frequency (cm^{-1}) for normal and oblique incidence: (a) experimental result at T = 5 K from Ref. 85 and (b) our theoretical calculation. The SL consisted of 25 repeat periods of 90-Å ZnTe and 45-Å CdSe.

spectra at oblique incidence. In the Raman backscattering, as the TO phonon is forbidden in the CdSe/GaAs (001) geometry, the value of $\omega_{TO} = 172$ cm^{-1} obtained from the transmission study has provided strong justification to the frequency deduced from the realistic lattice dynamics,[98] as well as MREI model (see Fig. 5) calculations. Moreover, the frequencies of the LO and TO phonons in CdSe are found to satisfy the Lyddane-Sachs-Teller relation ($\varepsilon_o/\varepsilon_\infty = \omega_{LO}{}^2/\omega_{TO}{}^2$).

Similar to the FIR transmission spectra, we display in Fig. 8 our results of the calculated reflectivity spectra at an oblique incidence ($\theta_i = 45^\circ$) for CdSe/GaAs (001) epilayers with increasing CdSe thickness. It should be borne in mind that in the binary semiconductors the reflectance spectra generally drop to a minimum at the plasma edge that is obviously dependent upon the carrier concentration and exhibit a peak near the TO phonon frequency. In a semi-insulating material with $\omega_p \approx 0$, (Eq. (2)), the ω_{TO} phonon peak dominates at near-normal incidence; at an oblique incidence ($\theta_i = 45^\circ$), a maxima is expected to occur at ω_{TO} and a dip near ω_{LO} (Berreman effect) is expected in the *p*-polarization reflectivity.[89] Extending the arguments from a free-standing film to an epilayer structure, our results of the reflectance study in CdSe/GaAs (001) clearly exhibited the major attributes of the CdSe and GaAs optical phonon energies. These results provided strong justifications for the polarized transmission and reflectivity studies being applied successfully to many technologically important thin multilayer structures for extracting useful information about ω_{TO}, ω_{LO} phonons in the individual layers (e.g., epitaxially semiconductor SLs grown on different substrates; c.f. Sec. IV B 3).

3. $(CdSe)_m/(ZnTe)_n$/GaAs (001) SLs

In this section, we demonstrate and confer our theoretical (c.f. Sec. III B) results of the transmission and reflectivity spectra for a $(CdSe)_m/(ZnTe)_n$ SL grown on GaAs (001) substrate. To contrast the simulated spectra at oblique incidence against the experimental transmission data, we examined the SL structure consisting of 25 repeat periods of 90 Å of ZnTe and 45 Å of CdSe grown on GaAs (001) substrate by MBE. The polarized FIR transmission spectra for the SL were obtained using a BOMEM DA.8 rapid scanning FTIR spectrometer.[85] The experimental data at oblique incidence displayed in Fig. 9 (a) compare fairly well with our calculated transmission spectra reported in Fig. 9 (b). Again, the transmission dips associated with CdSe and ZnTe at normal ($\theta_i = 0^\circ$) and oblique ($\theta_i = 45^\circ$) incidence provided strong corroboration to the values of ω_{TO} ($\equiv$171. 4 cm^{-1} CdSe; 181.8 cm^{-1} ZnTe) and ω_{TO}, ω_{LO} ($\equiv$211.3 cm^{-1} CdSe; 210.4 cm^{-1} ZnTe) phonons.[98] As the TO and LO modes in CdSe and ZnTe layers are separated by $\sim$10 and $\sim$1 cm^{-1}, respectively, the transmission minima occurring at appropriate frequencies with proper splitting elucidates the importance of

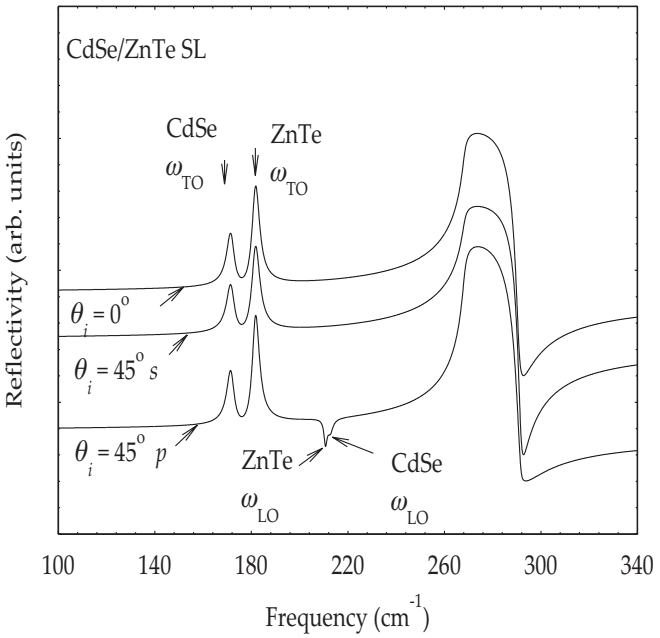

FIG. 10. Calculated reflectivity spectra for a CdSe/ZnTe SL grown on GaAs substrate as a function of frequency (cm^{-1}) for normal $\theta_i = 0^\circ$ and oblique incidence $\theta_i = 45^\circ$ (s- and p-polarization). The SL consisted of 25 repeat periods of 90-Å ZnTe and 45-Å CdSe.

the present methodology. Again, due to a small (∼0.76%) lattice mismatch between cubic CdSe and ZnTe, the shifts of optical phonon frequencies in the SL structure are found to be negligible compared to their "strain-free" phonon energy values.[98]

In Fig. 10, we present the results of our s- and p-polarized FIR reflectance calculations at normal ($\theta_i = 0^\circ$) and oblique ($\theta_i = 45^\circ$) incidence for the same $(CdSe)_m/(ZnTe)_n$/GaAs (001) SL structure used in the calculation of the transmission spectra (see Fig. 9). Consistent with the results displayed in Fig. 8, the reflectivity spectra for the SL structure exhibit two maxima at ω_{TO} near ∼171.4 and 181.8 cm^{-1} at normal ($\theta_i = 0^\circ$) and s-polarized oblique ($\theta_i = 45^\circ$) incidence related to the ω_{TO} modes of CdSe and ZnTe, respectively. In the p-polarized reflectivity spectra, in addition to the TO modes, we find two clearly visible dips (one pronounced and the other weak) near ∼210.4 and 211.3 cm^{-1} exhibiting the LO phonons of ZnTe and CdSe, respectively.

V. CONCLUSIONS

We have performed FIR reflectance measurements on a series of good optical-quality zinc-blende-type $Cd_xZn_{1-x}Te$ ($0 \leqslant x \leqslant 1$), $CdSe_xTe_{1-x}$ ($0 < x \leqslant 0.35$) material samples grown by Bridgman technique. In $Cd_xZn_{1-x}Te$ alloys, the composition-dependent spectra exhibited many fundamental aspects of the lattice vibrations, while the results of long-wavelength optical modes of the end members displayed zone-center phonon values in good agreement with the existing inelastic neutron[56] and/or Raman scattering[85] data. The optical phonons in the reflectance spectra of $CdSe_xTe_{1-x}$ ($0.35 \geqslant x > 0.05$) alloys, on the other hand, revealed a variety of behavior patterns depending upon the vibrational characteristics of the end members. Based on the calculations of density of states using Green's function theory, the unresolved phonon feature seen between CdSe-like and CdTe-like TO modes in $CdSe_xTe_{1-x}$ for ($x > 0.05$) is suggested to be originating from a nonrandom alloy disorder.[98] Simulation results of the FIR reflectance and transmission spectra at oblique incidence (Berreman's effect) are presented for a variety of II-VI free-standing thin films, epilayers, and SLs using a standard methodology of multilayer optics ($d \ll \lambda$) with effective-medium dielectric tensors. For cubic CdTe, CdSe, and ZnTe thin films, the values of optical phonons extracted by the Berreman technique are found in very good agreement with the existing data from inelastic neutron scattering and Raman spectroscopy. Comparison of the calculated transmission spectra for the $(CdSe)_m/(ZnTe)_n$/GaAs (001) SL not only has provided an excellent accord with the experimental results but also has revealed distinctive minima associated with the appropriate phonons of CdSe and ZnTe. In conclusion, the Berreman method has provided a strong basis for analyzing the IR experimental data at oblique incidence and offered an effective means of estimating the zone-center TO and LO (ω_{TO} and ω_{LO}) phonon frequencies in polar-semiconductor thin films and heterostructure materials of increasing technological importance.

ACKNOWLEDGMENTS

D.N.T. acknowledges useful discussions on the subject matter with M. D. Tiwari of the Indian Institute of Information Technology, Allahabad, India, and an Innovation Grant received from the School of Graduate Studies at Indiana University of Pennsylvania. The work at the National Taiwan University was supported by Grants No. NSC 98-2221-E-002-015-MY3 and No. NSC 98-3114-E-005-002-CC2. We also acknowledge technical help in graphing.

*talwar@iup.edu

[1] S. Adachi, *Properties of Semiconductor Alloys*, Wiley Series in Materials for Electronic and Optoelectronic Applications (Wiley, 2009), Ch. 4, p. 99.

[2] W. J. Min, J. Sunghan, J. L. Sung, K. Yongwook, and S. S. Koo, J. Phys. Chem. A **113**, 9588 (2009).

[3] T. Park, J. Lee, W. Lee, J. Ahn, and W. Yi, in *22nd International Vacuum Nanoelectronics Conference* (Shizuoka, Japan, 2009), p. 275.

[4] C. Reig, M.-D. Cubells-Beltrán, and D. Ramírez Muñoz, Sensors **9**, 7919 (2009).

[5] M. B. Reine, in *Proceedings of the SPIE*, Vol. 7298 (Orlando, Florida, May 7, 2009).

[6] M. M. Crouse, T. L. James, and D. Crouse, in *SPIE Proceedings Nanophotonics and Macrophotonics for Space Environments II*, edited by E. W. Taylor and D. A. Cardimona, Vol. 7095 (San Diego, CA, August 25, 2008).

[7] P. V. Kamat, J. Phys. Chem. C **112**, 18737 (2008).

[8] S. K. Shin, H.-J. Yoon, Y. J. Jung, and J. W. Park, Curr. Opin. Chem. Biol. **10**, 423 (2006).

[9] P. Swaminathan, V. N. Antonov, J. A. N. T. Soares, J. S. Palmer, and J. H. Weaver, Phys. Rev. B **73**, 125430 (2006).

[10] M. C. Gupta and J. Ballato, Eds. *Handbook of Photonics* (Taylor and Francis, New York, 2006).

[11] A. Rogalski, Opto-electron. Rev. **14**, 87 (2006).

[12] M. C. Tamargo, Ed. *II-VI Semiconductor Materials and Their Applications (Optoelectronic Properties of Semiconductors and Superlattices*, Vol. 12 (Taylor Francis, 2001).

[13] S. Stepanov, in *Handbook for Advanced Electronic and Photonic Materials and Devices*, edited by H. S. Nalwa, Vol. 2 (Academic Press, 2001), Ch. 6, p. 205.

[14] H. Ruda, Ed. *Widegap II-VI Compounds for Optoelectronic Applications* (Chapman and Hill, London, 1992), p. 415.

[15] G. E. Hallani, A. Ryah, N. Hassanain, M. Loghmarti, A. Mzerd, A. Arbaoui, N. Achargui, Y. Laaziz, N. Chahboun, and E. K. Hlil, in *Progress in Electromagnetics Research Symposium*, (Marrakesh, Morocco, 2011) p. 1897.

[16] H. Qiao, B. Guan, T. Böcking, M. Gal, J. J. Gooding, and P. J. Reece, Appl. Phys. Lett. **96**, 161106 (2010).

[17] C. Reig, C. Gómez-García, and S. V. Muñoz, Microelectron. J. **38**, 327 (2007).

[18] I. L. Medintz, H. T. Uyeda, E. R. Goldman, and H. Mattoussi, Nat. Mater. **4**, 435 (2005).

[19] X. Michalet, F. F. Pinaud, L. A. Bentolila, J. M. Tsay, S. Doose, J. J. Li, G. Sundaresan, A. M. Wu, S. S. Gambhir, and S. Weiss, Science **307**, 538 (2005).

[20] I. Hernández-Calderón, M. García-Rocha, and P. Díaz-Arencibia, Phys. Status Solid. B **241**, 558 (2004).

[21] X. Liu and J. K. Furdyna, J. Appl. Phys. **95**, 7754 (2004).

[22] Y. Luo, S. P. Guo, O. Maksimov, M. C. Tamargo, V. Asnin, F. H. Pollak, and Y. C. Chen, Appl. Phys. Lett. **77**, 4259 (2000).

[23] A. Salokatve, K. Rakennus, P. Uusimaa, M. Pessa, T. Aherne, J. P. Doran, J. O'Gorman, and J. Hegarty, Appl. Phys. Lett. **67**, 407 (1995).

[24] L. A. Kolodziejski, R. L. Gunshor, and A. V. Nurmikko, Annu. Rev. Matter. Sci. **25**, 711 (1995).

[25] Z. Yu, D. B. Eason, C. Boney, J. Ren, W. C. Hughes, W. H. Rowland Jr., J. W. Cook Jr., J. F. Schetzina, G. Cantwell, and W. C. Harsch, J. Vac. Sci. Technol. B **13**, 711 (1995).

[26] S. Permogorov and A. Reznitsky, J. Lumin. **52**, 201 (1992).

[27] A. Tu and P. D. Persans, Appl. Phys. Lett. **58**, 1506 (1991).

[28] I. V. Sedova, S. V. Sorokin, A. A. Sitnikova, R. V. Zolotaveva, S. V. Ivanov, and P. S. Kop'ev, in *7th International Symposium on Nanostructure "Physics and Technology"* (St. Petersburg, Russia, 1999), [http://handle.dtic.mil/100.2/ADP012998].

[29] S. V. Ivanov, A. A. Toropov, S. V. Sorokin, T. V. Shubina, N. D. Il'inskaya, A. V. Lebedev, I. V. Sedova, P. S. Kop'ev, Zh. I. Alferov, H.-J. Lugauer, G. Reuscher, M. Keim, F. Fischer, A. Waag, and G. Landwehr, Semiconductors **32**, 1137 (1998).

[30] L. H. Kuo, L. Salamanca-Riba, B. J. Wu, G. M. Haugen, J. M. DePuydt, G. Hofler, and H. Cheng, J. Vac. Sci. Technol. B **13**, 1694 (1995).

[31] L. Worschech, W. Ossau, W. Behr, Th. J. Nurnberger, and G. Landwehr, Appl. Phys. Lett. **73**, 835 (1998).

[32] H. Jeon, J. Ding, A. V. Nurmikko, W. Xie, D. C. Grillo, M. Kobayashi, R. L. Gunshor, G. C. Hua, and N. Otsuka, Appl. Phys. Lett. **60**, 2045 (1992).

[33] M. M. Zverev, D. V. Peregudov, I. V. Sedova, S. V. Sorokin, S. V. Ivanov, and P. S. Kop'ev, Quant. Electron. **34**, 909 (2004).

[34] P. Kuznetsov[1], V. Lusanov, G. Yakushcheva, V. Jitov, L. Zakharov, I. Kotelyanskii, and V. Kozlovsky, Phys. Status Solid. C **7**, 1568 (2010).

[35] J. J. Coleman, in *Proceedings of the IEEE*, Vol. 85, Nov. 1997, p. 1715; A. G. Thompson, Mater. Lett. **30**, 255 (1997).

[36] J. Huerta, M. López, and O. Zelaya, Superficies y Vacio **8**, 125 (1999).

[37] L. C. Calhoun and R. M. Park, J. Appl. Phys. **85**, 490 (1999).

[38] J. S. Foord, G. J. Davies, and W. T. Tsang, Eds. *Chemical Beam Epitaxy and Related Techniques* (Wiley, 1997).

[39] M. Hetterich, M. Grün, H. Gerlach, and C. Klingshirn, Mater. Sci. Forum **182-184**, 415 (1995).

[40] W. Shan, S. J. Hwang, J. M. Hays, J. J. Song, Z. Q. Zhu, and T. Yao, J. Appl. Phys. **74**, 5699 (1993).

[41] F. Gindele, U. Woggon, W. Langbein, J. M. Hvam, K. Leonardi, D. Hommel, and H. Selke, Phys. Rev. B **60**, 8773 (1999).

[42] O. de Melo, C. Vargas, and I. Hernandez-Calderon, Appl. Phys. Lett. **82**, 43 (2003).

[43] K. Ichino, Y.-H. Wu, Y. Kawakami, S. Fujita, and S. Fujita, J. Cryst. Growth **117**, 527 (1992).

[44] M. J. S. P. Brasil, R. E. Nahory, F. S. Turco-Sandroff, H. L. Gilchrist, and R. J. Martin, Appl. Phys. Lett. **58**, 2509 (1991).

[45] M. J. S. P. Brasil, M. C. Tamargo, R. E. Nahory, H. L. Gilchrist, and R. J. Martin, Appl. Phys. Lett. **59**, 1206 (1991).

[46] N. Samarth, H. Lou, J. K. Furdyna, S. B. Qadri, Y. R. Lee, A. K. Ramdas, and N. Otsuka, Appl. Phys. Lett. **54**, 2680 (1989).

[47] O. de Melo, E. Sanchez, H. Rodriguez, S. de Roux, F. Rabago-Bernal, and J. Rouiz-Garcia, Mater. Chem. Phys. **59**, 120 (1999).

[48] F. Zhang, Z. He, and C. E. Seifert, IEEE Trans. Nucl. Sci. **54**, 843 (2007).

[49] K.-O. Kim, J. K. Kim, J.-H. Ha, and S. Y. Kim, Nucl. Eng. Tech. **41**, 723 (2009).

[50] K. Parnham, C. Szeles, T. H. Prettyman, M. Smith, B. H. Parker, C. Stahle, L. L. Wang, [http://www.evmicroelectronics.com/pdf/Applications/Further%20Studies.pdf].

[51] L. Abbene, S. Del Sordo, E. Caroli, G. Gerardi, G. Raso, S. Caccia, and G. Bertuccio, J. Appl. Phys. **105**, 124508 (2009).

[52] W. Li, L. Huan Feng, J. Q. Zhang, L. L. Wu, Y. P. Cai, J. G. Zheng, W. Cai, B. Li, and Z. Lei, Sci. China E **51**, 33 (2008).

[53] R. Dhere, T. Gessert, J. Zhou, S. Asher, J. Pankow, and H. Moutinho, in *Materials Research Society Spring Meeting* (San Francisco, California, 2003).

[54] A. Morales-Acevedo, in *25th European Photovoltaic Solar Energy Conference and Exhibition/5th World Conference on Photovoltaic Energy Conversion* (Valencia, Spain, 2010).

[55] G. Sivaraman, M.S. Thesis, University of South Florida, Nov. 12, 2003.

[56] J. M. Rowe, R. M. Nicklow, D. L. Price, and K. Zanio, Phys. Rev. B **10**, 671 (1974); N. Vagelatos, D. Wehe, and J. S. King, J. Chem. Phys. **60**, 3613 (1974).

[57] J. C. Irwin and J. LaCombe, J. Appl. Phys. **45**, 567 (1974).

[58] P. Plumelle and M. Vandevyver, Phys. Status Solid. B **73**, 271 (1976).

[59] M. Kitamura, S. Muramatsu, and W. A. Harrison, Phys. Rev. B **46**, 1351 (1992).

[60]A. DalCorso, S. Baroni, R. Resta, and S. deGironcoli, Phys. Rev. B **47**, 3588 (1993).
[61]O. Zakharov, A. Rubio, X. Blasé, M. L. Cohen, and S. G. Louie, Phys. Rev. B **50**, 10780 (1994).
[62]B. D. Rajput and D. A. Browne, Phys. Rev. B **53**, 9052 (1996).
[63]M. Cotè, O. Zakharov, A. Rubio, and M. L. Cohen, Phys. Rev. B **55**, 13025 (1997).
[64]S. H. Wei and S. B. Zhang, Phys. Rev. B **62**, 6944 (2000).
[65]A. Mujica, A. Rubio, A. Munoz, and R. J. Needs, Rev. Mod. Phys. **75**, 863 (2003).
[66]E. Deligoz, K. Colakoglu, and Y. Ciftci, Phys. B **373**, 124 (2006).
[67]N. Jabari Lee, R. K. Kalia, A. Nakano, and P. Vashishta, Appl. Phys. Lett. **89**, 093101 (2006).
[68]S. Q. Wang, Mater. Sci. Forum **561**, 1907 (2007).
[69]A. Erçelebi and R. T. Senger, Phys. Rev. B **53**, 11008 (1996).
[70]A. Leitenstorfer and A. Laubereau, Semicond. Semimet. **67**, 1 (2001).
[71]M. I. Vasilevskiy, E. V. Anda, and S. S. Makler, Phys. Rev. B **70**, 035318 (2004).
[72]R. T. Senger and K. K. Bajaj, Phys. Status Solid. B **241**, 1896 (2004).
[73]E. M. Sheregii, J. Cebulskii, A. Marcelli, and M. Piccinini, Chin. J. Phys. **49**, 214 (2011).
[74]H. Narada and S. Narita, J. Phys. Soc. Jpn. **30**, 1628 (1970).
[75]L. K. Vodopyanov, E. A. Vinogradov, A. M. Blinov, and V. A. Rukavishnikov, Sov. Phys. Solid State **14**, 219 (1972).
[76]M. Gorska and W. Nazarewicz, Phys. Status Solid. B **57**, K65 (1973); **65**, 193 (1974).
[77]E. A. Vinogradov, L. K. Vodopyanov, and G. S. Oleinik, Sov. Phys. Solid State **15**, 322 (1973).
[78]E. A. Vinogradov and L. K. Vodopyanov, Sov. Phys. Solid State **17**, 2088 (1976).
[79]V. G. Plotnichenko, L. V. Golubev and L. K. Vodopyanov, Sov. Phys. Solid State **19**, 1582 (1977).
[80]M. Macler, Z. C. Feng, S. Perkowitz, R. Rousina, and J. Webb, Phys. Rev. B **46**, 6902 (1992).
[81]R. Granger, Y. Marqueton, and R. Triboulet, J. Phys. **3**, 135 (1993).
[82]D. W. Berreman, Phys. Rev. **130**, 2193 (1963).
[83]J. Ibáñez, S. Hernández, E. Alarcón-Lladó, R. Cuscó, L. Artús, S. V. Navikov, C. T. Foxon, and E. Calleja, J. Appl. Phys. **104**, 033544 (2008).
[84]J. Ibáñez, E. Tarhan, A. K. Ramdas, S. Hernández, R. Cuscó, L. Artús, M. R. Melloch, and M. Hopkinson, Phys. Rev. B **69**, 075314 (2004).
[85]M. D. Sciacca, A. J. Mayur, E. Oh, A. K. Ramdas, S. Rodriguez, J. K. Furdyna, M. R. Melloch, C. P. Beetz, and W. S. Yoo, Phys. Rev. B **51**, 7744 (1995).
[86]E. Oh, A. K. Ramdas, T. Fromherz, W. Faschinger, G. Bauer, and H. Sitter, Phys. Rev. B **48**, 17364 (1993); T. Fromherz, E. Oh, A. K. Ramdas, E. Koppensteiner, G. Bauer, W. Faschinger, and H. Sitter, J. Cryst. Growth **138**, 580 (1994).
[87]V. S. Vinogradov, G. Karczewski, I. V. Kucherenko, N. N. Mel'nik, and P. Fernandez, Phys. Solid State **50**, 164 (2008).
[88]A. I. Belogorokhov, I. A. Denisov, N. A. Smirnova, and L. I. Belogorokhova, Semiconductors **38**, 82 (2004); A. I. Belogorokhov, N. A. Smirnova, I. A. Denisov, L. I. Belogorokhova, and B. N. Levonovich, Phys. Stat. Solid. C **7**, 1624 (2010).
[89]A. Silva-Castillo and F. Pérez-Rodŕiguez, J. Appl. Phys. **86**, 1404 (1999).
[90]E. A. Vinogradov, B. N. Mavrin, N. N. Novikova, V. A. Yakovlev, and D. M. Popova, Laser Phys. **19**, 162 (2009).
[91]K. Kunc, Ann. Phys. **8**, 319 (1973–74).
[92]D. N. Talwar, M. Vandevyver, K. Kunc, and M. Zigone, Phys. Rev. B **24**, 741 (1981).
[93]D. N. Talwar, Z. C. Feng, and P. Becla, Phys. Rev. B **48**, 17064 (1993).
[94]D. N. Talwar, B. Roughani, J. G. Pellegrino, P. Amirtharaj, and S. B. Qadri, Mater. Sci. Eng. B **44**, 143 (1997).
[95]D. N. Talwar, in *Dilute III-V Nitride Semiconductors and Material Systems—Physics and Technology*, Springer Series in Materials Science 105, edited by A. Erol (Springer-Verlag, 2008), Chap. 9, p. 222.
[96]D. N. Talwar, Appl. Phys. Lett. **97**, 051902 (2010).
[97]D. N. Talwar, Phys. Rev. B **82**, 085207 (2010).
[98]D. N. Talwar (unpublished).
[99]Z. C. Feng, P. Becla, L. S. Kim, S. Perkowitz, Y. P. Feng, H. C. Poon, K. M. Williams, and G. D. Pitt, J. Cryst. Growth **138**, 239 (1994); T.-R. Yang, S.-H. Jhang, F.-C. Hou, Y.-C. Yang, P. Becla, D.-C. Tien, and Z. Chuan Feng, in *Proceedings of the SPIE*, Vol. 7499 (San Diego, California, Aug. 2009).
[100]T. W. Cadman and D. Sadowski, Appl. Opt. **17**, 531 (1978).
[101]O. E. Piro, Phys. Rev. B **36**, 3427 (1987).
[102]O. Pag̀es, T. Tite, K. Kim, P. A. Graf, O. Maksimov, and M. C. Tamargo, J. Phys. Condens. Matter **18**, 577 (2006).